LETTER

Indentation and contact damages on grain boundary controlled silicon carbide ceramics

Rae Hyeong Ryu · Kee Sung Lee · Young-Wook Kim

Silicon carbide (SiC) ceramics have been studied with particular interest for engineering applications that require high wear resistance [1–4]. The high hardness of SiC ceramics is accompanied by wear, erosion, and mechanical fatigue resistance. Considerable resistance in corrosive environments such as plasma-enhanced environments is required for hard SiC ceramics in the semiconductor industry. In these materials, mechanical contact is one of the important considerations in the lifetimes of components [5, 6]. The surfaces of the material can be subjected to contact loads ranging, from single to multiple concentrated loads. Thus, reduced sensitivity against the damages— "flaw tolerance" or "damage tolerance"—is required to prolong the lifetimes of the components in service [7–10].

While SiC ceramics exhibit excellent wear resistance, the critical drawback is low reliability due to the inferior fracture toughness. Therefore, over several decades, studies have demonstrated that the toughness properties of SiC can be improved by a heterogeneous microstructure with weak grain boundary phases [3, 11–13]. Those microstructures can be obtained via liquid phase sintering that uses metal oxides, Al–B–C, Y_2O_3–Al_2O_3 [14, 15], or AlN–metal oxide as the sintering additives. These additives form a melt at relatively low temperature and remain at the grain boundaries in the form of an amorphous intergranular film and/or at the ternary junctions after sintering. On the other hand, some compositions such as AlN–Sc_2O_3 and AlN–

R. H. Ryu · K. S. Lee (✉)
School of Mechanical and Automotive Engineering,
Kookmin University, Seoul 136-702, Korea
e-mail: keeslee@kookmin.ac.kr

Y.-W. Kim
Department of Materials Science and Engineering,
The University of Seoul, Seoul 130-743, Korea

Lu_2O_3, resulted in amorphous-free SiC ceramics [16]. They exhibit almost clean boundaries without amorphous grain phases as well as crystallized boundaries [17].

The purpose of this study is to investigate the effect of grain boundary compositions on the indentation properties of advanced SiC material that have high hardness. We used Hertzian and Vickers indentation that are simple techniques for inducing contact damage on the flat surface. A hard indenter is pressed on the surface of the specimen, and the damage patterns are examined [11]. In particular, in the present study, we investigate the effect of the grain boundary on the contact resistance of SiC ceramics.

In this work, different sintering additives were used during sintering; 1.8 wt% AlN and 9.6 wt% Sc_2O_3, 2.7%wt% AlN and 17.9 wt% Lu_2O_3, or 2.9 wt% AlN and 10.6 wt% Y_2O_3. All compositions have 10 vol.% of sintering additives. Mechanical properties such as hardness and fracture toughness are investigated by Vickers indentation. The contact damages and radial cracks are observed. We also characterize the damage by Hertzian indentation with spherical indenters. The characterizations are conducted on three SiC ceramics with similar microstructures (typical elongated microstructures).

The starting powders for grain boundary controlled SiC ceramics for characterizing mechanical properties and contact damages were α-SiC (A-1 grade, Showa Denko, Tokyo, Japan), β-SiC (Ultrafine grade, Betarundum, Ibiden Co. Ltd., Ogaki, Japan), AlN (Grade F, Tokuyama Soda Co, Tokyo, Japan), Sc_2O_3, Lu_2O_3, and Y_2O_3 (99.9% of purity, Shin-Etsu Chemical Co., Tokyo, Japan). 1 vol.% of α-SiC is added to 99 vol.% β-SiC to develop a self-reinforced coarse and elongated microstructure. The detailed starting compositions of SiC + AlN + Sc_2O_3, SiC + AlN + Lu_2O_3, and SiC + AlN + Y_2O_3 are described in Table 1. Throughout the paper, SiC sintered with AlN and

Sc_2O_3, SiC sintered with AlN and Lu_2O_3 and SiC sintered with AlN and Y_2O_3 are designated by **SC1**, **SC2**, and **SC3**, respectively. Each batch of powder shown in Table 1 was mixed as slurry in ethanol for 24 h in a planetary ball mill, using SiC grinding balls. The milled powder was dried and sieved. Then each composition of powder was hot-pressed at 1,900 °C for 1 h under a uniaxial pressure of 25 MPa in N_2 atmosphere. The hot-pressed specimens were further annealed at 2,000 °C for 6 h with an applied pressure of 25 MPa.

The sintered densities were measured through the Archimedes method. The phase of sintered products was qualitatively analyzed through an X-ray diffractometer after the ground powders were prepared for the annealed specimens. The hot-pressed and annealed specimens were cut and polished, and then etched by a plasma of CF_4 that contained 10% O_2. The microstructure and the morphology of the fractured section were examined by scanning electron microscopy (SEM, JEOL, JSM-6700F, Japan).

The surface of each specimen was ground, cut into 3 mm × 4 mm × 5 mm bars, and polished to 1 μm finish to enable characterization and indentation testing. Hertzian indentations [18–23] were made using tungsten carbide spheres of radius $r = 1.98$ mm, over a load range $P = 0$–1,000 N using a universal testing machine (Model 5567, Instron, USA). Vickers indentation tests were performed by using a microhardness tester. A conventional Vickers indentation was performed to measure the hardness and toughness, at loads of $P = 20$–100 N, on the polished surfaces. Ten indents were performed under the same loading condition. After indentation, FE-SEM was used to examine the surface deformation and damages, from a surface view and crack propagations around the indentation sites.

X-ray diffraction analysis revealed that all the SiC ceramics, **SC1**, **SC2**, and **SC3**, consist of major peaks of α-SiC and minor peaks of β-SiC. Crystalline phases of $Sc_2Si_2O_7$, Sc_2SiO_5, $Lu_2Si_2O_7$, and $Y_2Si_2O_7$ are found depending upon the sintering additives, respectively. The results are summarized in Table 1. The relative densities of **SC1**, **SC2**, and **SC3** that are sintered at 1,900°C for 1 h and annealed at 2,000 °C for 6 h are shown in Table 1. The sintered densities of bulk material were measured, and the calculated relative densities are summarized in the table. The result indicates that relative densities of ≥98% were achieved for all the compositions by hot-pressing and subsequently annealing the specimens. The AlN–Sc_2O_3, AlN–Lu_2O_3, or AlN–Y_2O_3 additives react with the SiO_2 that is on the surface of SiC, and form an oxycarbonitride melt through the dissolution of SiC with increasing temperature.

Microstructures of polished and etched surfaces of **SC1**, **SC2**, and **SC3** are shown in Fig. 1. The microstructure was observed by scanning electron microscopy (SEM). All specimens contain the same total amount of additives (10 vol.%), but have different compositions. All the specimens show similar microstructures, which consist mainly of elongated α phases and minor β phases. The development of elongated grains in the specimens results from β to α phase transformation during sintering and annealing. Previous studies [16] on the high resolution TEM images of **SC1**, **SC2**, and **SC3** along the SiC–SiC grain boundaries indicate that almost clean grain boundaries without any amorphous grain boundary films were observed in **SC1** while crystallized and amorphous boundaries were observed in **SC2** and **SC3**, respectively. The thicknesses of the crystallized boundary in **SC2** are ∼1 nm and those of the amorphous boundary in **SC3** are ∼4.4 nm. The sintering additives of **SC3** react with the SiO_2 that exist on the surface of SiC to form an amorphous phase at a relatively low temperature. This contributes to the liquid phase sintering of SiC ceramics and remains in the form of intergranular grain boundary film. The refined continuum model predicts that the incorporation of cations with smaller size into silica glass leads to almost clean boundaries [16, 17]. In the case of **SC2**, it seems that the composition of the sintering additives plays a dominant role in the evolution of crystalline grain boundary structures during annealing.

Since Hertz first investigated the cone-shaped fractures that are produced through contact between glass lenses, indentation mechanics has been used in the analysis and

Table 1 Characteristics of the sintered and annealed SiC specimens

Specimen designation	Batch composition (wt%)	Relative density (%)	Crystalline phase			Interface phase[a]	Grain boundary thickness (nm)[a]
			Major	Minor	Trace		
SC1	87.7% β-SiC + 0.9% α-SiC + 1.8%AlN + 9.6% Sc_2O_3	98.1	α-SiC	β-SiC	$Sc_2Si_2O_7$ Sc_2SiO_5	Almost clean phase	∼0
SC2	78.6% β-SiC + 0.8% α-SiC + 2.7% AlN + 17.9% Lu_2O_3	98.3	α-SiC	β-SiC	$Lu_2Si_2O_7$	Crystalline phase	∼1
SC3	85.6% β-SiC + 0.9% α-SiC + 2.9% AlN +10.6% Y_2O_3	98.3	α-SiC	β-SiC	$Y_2Si_2O_7$	Amorphous phase	∼4.5

[a] The results of characteristics are from reference [16]

Fig. 1 Typical microstructures of SiC ceramics: **a** SC1, **b** SC2, and **c** SC3
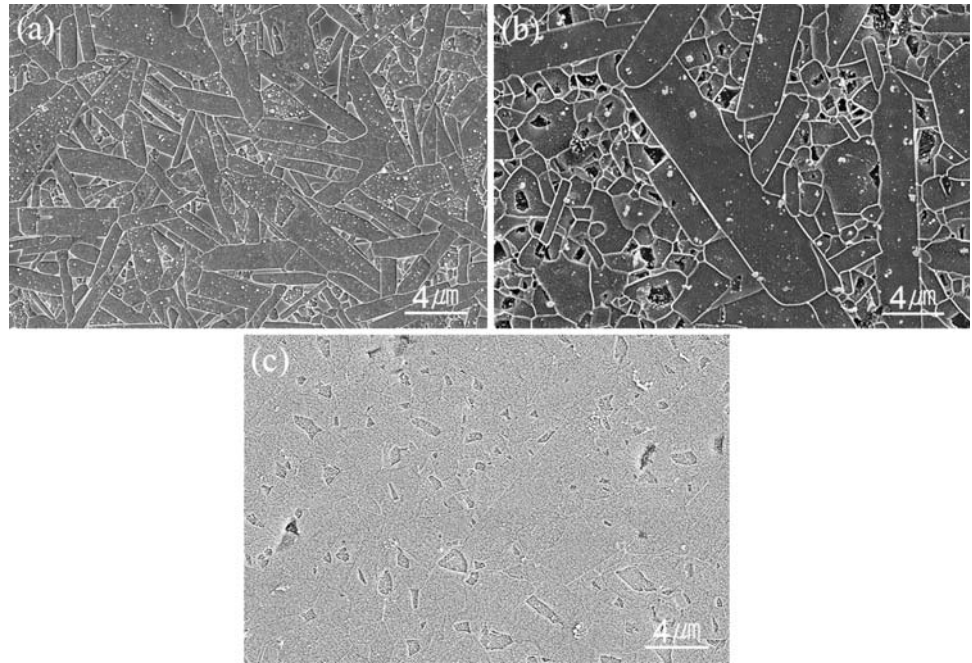
mechanical characterization of ceramics [5, 24, 25]. Contact damage by Hertzian indentation is recognized as a key limiting factor in the lifetime of ceramics in many engineering applications [5, 24–26]. The surface views of the contact damage by spherical indentation in the grain boundary controlled **SC1**, **SC2**, and **SC3** ceramics under the contact load at $P = 1,000$ N using WC sphere $r = 1.98$ mm are shown in Fig. 2. Full ring cracks are apparent for **SC3**,

while partial ring cracks are seen in the surface of **SC1**. The crack of **SC2** has propagated more than that of **SC1**. The initiation of ring cracks, P_{cone}, can be modeled [5, 11], by the following equation for cone cracking:

$$P_{cone} = A\, r\, G_c. \tag{1}$$

In Eq. 1, G_c is the crack resistance, r the radius of indenter, and A a dimensionless constant. The optical

Fig. 2 Hertzian indentation damage on the surface of **a** SC1, **b** SC2, and **c** SC 3 at a load of $P = 1,000$ N using WC sphere $r = 1.98$ mm
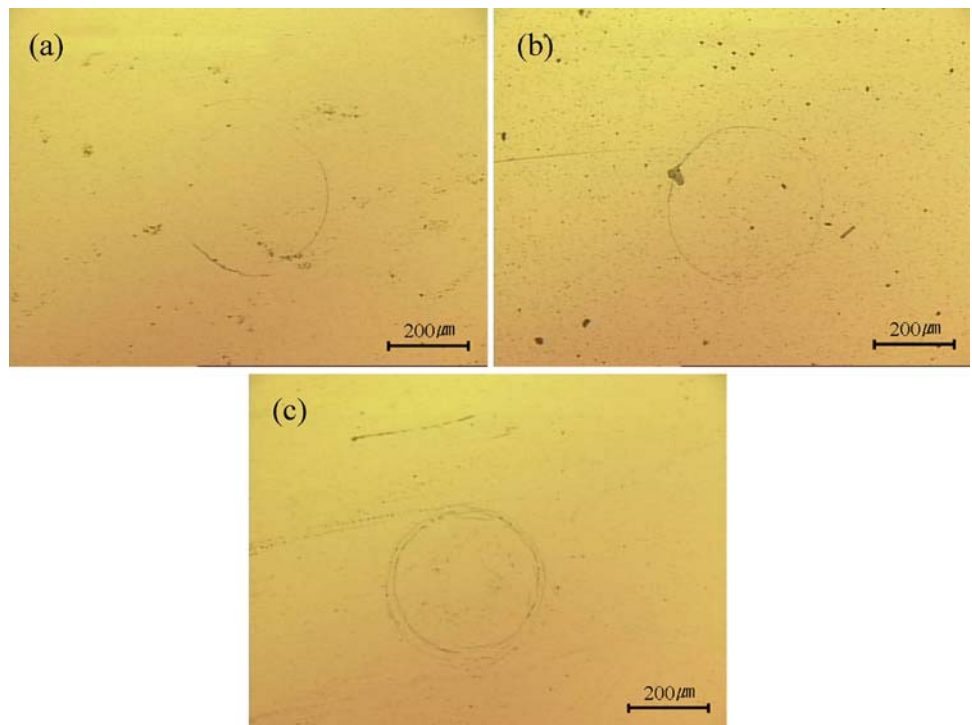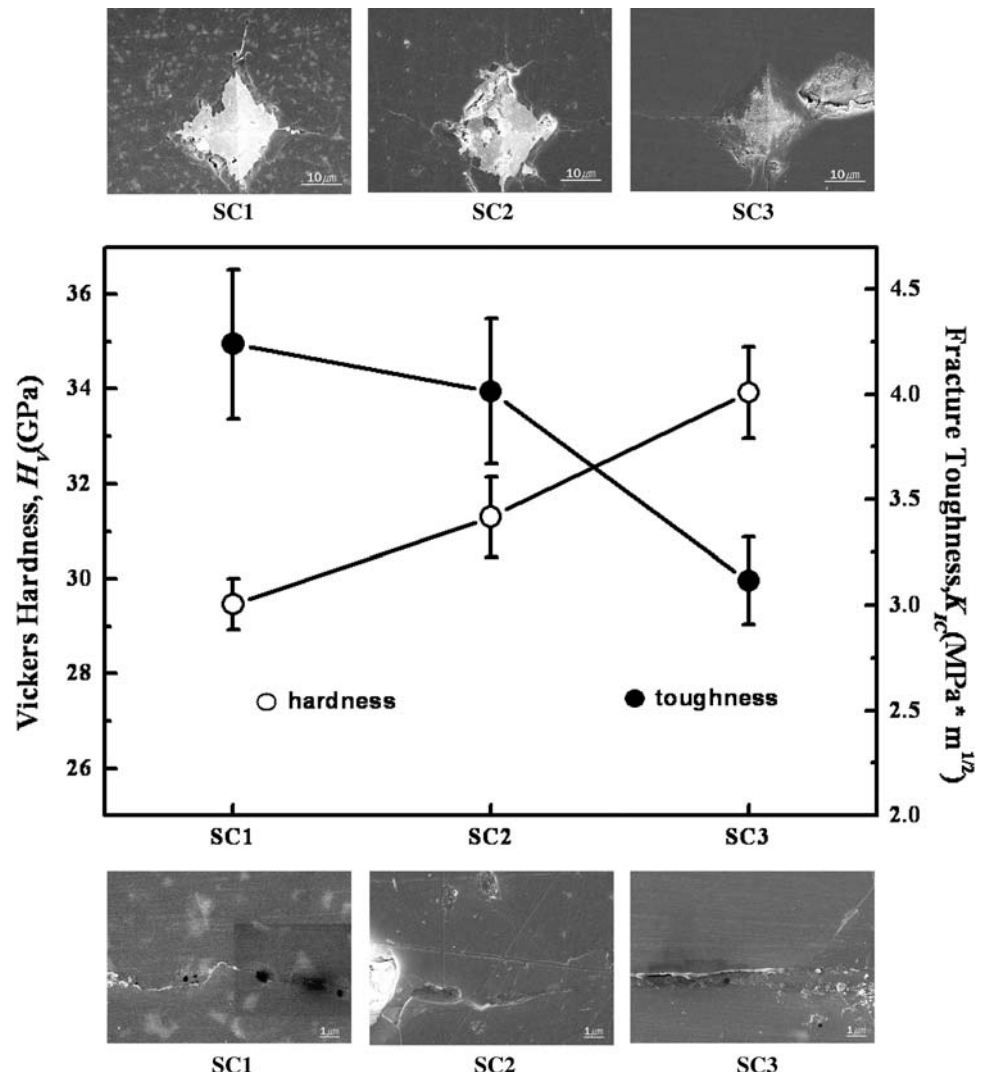
Fig. 3 Hardness and fracture toughness of **SC1**, **SC2**, and **SC3** at a load of $P = 20$ N. SEM views of Vickers indentation damage and cracks are inserted in the graph

micrographs of the surface as shown in Fig. 2 indicate that relatively extensive damage including multiple cracks, are apparent for **SC3**, while **SC1** exhibits lesser contact damage, indicating a greater resistance of **SC1** to cracks, as shown in Eq. 1. The result in Fig. 2 suggests that contact cracking and damages through indentation crucially depends upon the grain boundary composition in SiC ceramics.

Previous research has shown that quasi-plastic damages are apparent for SiC that is sintered with an Al_2O_3–Y_2O_3 additive [21]. The quasi-ductile surface impressions are usually observed in the liquid phase sintered SiC that consist of coarse and elongated grains [7]. However, in the present study, the grain boundary controlled **SC1**, **SC2**, and **SC3** ceramics represent brittle ring cracks compared to a quasi-plastic surface impression. Therefore, it is expected that the grain boundary controlled **SC1**, **SC2**, and **SC3** ceramics have greater wear and fatigue resistance due to the absence of quasi-plastic damage [9, 12, 23, 27].

The graph in Fig. 3 shows the hardness and the toughness of the grain boundary controlled **SC1**, **SC2**, and **SC3** ceramics. Commensurate with the trend of ring crack propagation in Fig. 2, the fracture toughness strongly falls off through the sequence **SC1**–**SC2**–**SC3**. Conversely, the hardness strongly increases through the sequence **SC3**–**SC2**–**SC1**. In this study, the **SC3** material is the hardest material, ~ 34 GPa. However, the hardness of **SC1** is still high, ~ 29.5 GPa, relative to that of liquid phase sintered SiC ceramics that are sintered with an Al_2O_3–Y_2O_3 additive, ~ 25 GPa [9, 12, 27]. The **SC1** material is the toughest material even though it is less hard than **SC2** and **SC3**. The fracture toughness of **SC1** was 4.2 MPa m$^{1/2}$. Note that the relative differences in the hardness and toughness are considerably greater when we consider that all SiC ceramics show similar microstructures as shown in Fig. 1, and similar densities and phases, except for the grain boundary composition, as indicated in Table 1. The

result means that grain boundary composition is a key factor that impacts the mechanical properties.

The discrepancies in the hardness can be understood by examination of the indentation impression damage, the views of which are inserted in the top three micrographs of Fig. 3. The micrographs represent top views of the damage that is formed at an indentation load of $P = 20$ N on the **SC1**, **SC2**, and **SC3** materials using a Vickers microhardness tester. Smaller indentation flaws are observed with radial cracks for **SC3**. It is thought that the discrepancy of the hardness in this study is related to dislocation movement during Vickers indentation. An amorphous grain boundary phase is accompanied by an increase in hardness, as the dislocation that is generated by the Vickers indenter is blocked by the amorphous phase, when compared to the crystalline or free phases [28]. However, on the whole, the hardness of the grain boundary controlled SiC ceramics investigated in this study showed very high values, ≥ 30 GPa. Observations were also made of radial cracks at Vickers indentations in the FE-SEM to determine the fracture pattern of the grain boundary controlled **SC1**, **SC2**, and **SC3** materials. The SEM views of cracks in the **SC1**, **SC2**, and **SC3** materials are inserted in the bottom three micrographs of Fig. 3. In **SC3**, the crack is relatively straight, with no indication of crack resistance. By contrast, the crack in **SC1** follows a deflected path. The propagation of the crack depends upon the grain boundary that arises from the addition of sintering additives with different compositions. It is thought that the discrepancy of the crack profiles are based on the residual stresses that originate from the mismatch in thermal expansion between SiC and grain boundary materials [29, 30].

In this study, 10 vol.% of Sc_2O_3–AlN, Lu_2O_3–AlN, or Y_2O_3–AlN sintering additives were added to SiC ceramics, to control the grain boundary, and thus, improve the mechanical properties and resistance to contact damage. Mechanical properties such as hardness and fracture toughness were measured, and Hertzian and Vickers indentation damage was investigated.

The results indicate that the hardness and toughness properties are influenced by the grain boundary; lower hardness and greater toughness for **SC1**, greater hardness and lower toughness for **SC3**, and mid-range values for **SC2**. The nature of the contact damage exhibited classical ring cracks that formed in a region of weak tension outside the contact, compared to microcracks in the diffuse quasi-plastic zones, as observed in the same heterogeneous microstructure of Al_2O_3–Y_2O_3 added SiC ceramics [12, 21]. This study suggests the control of the grain boundary compositions can improve the hardness. The greatest hardness of 34 GPa was found in SiC that was sintered with Y_2O_3–AlN. All the compositions in this study showed high hardness, ≥ 30 GPa.

References

1. Lange FF (1975) J Mater Sci 10:314. doi:10.1007/BF00540356
2. Mulla MA, Krstic VD (1991) Am Ceram Soc Bull 70:439
3. Ashcroft W (1975) Speical ceramics 6. Academic Press, New York
4. Kim YW, Chun YS, Nishimura T, Mitomo M, Lee YH (2007) Acta Mater 55:727
5. Lawn BR (1993) Fracture of brittle solids, chap 8, 2nd edn. Cambridge University Press, Cambridge
6. Yeo JG, Lee KS, Lawn BR (2000) J Am Ceram Soc 83:1545
7. Bennison SJ, Padture NP, Runyan JL, Lawn BR (1991) Phil Mag Lett 64:191
8. Braun LM, Bennison SJ, Lawn BR (1992) Composites and advanced ceramic materials, vol 13. American Ceramic Society, Ohio, p 156
9. Padture NP, Bennison SJ, Chan HM (1993) J Am Ceram Soc 76:2312
10. Lee SK, Lawn BR (1998) J Am Ceram Soc 81:997
11. Lawn BR (1998) J Am Ceram Soc 81:1977
12. Padture NP, Lawn BR (1994) J Am Ceram Soc 77:2518
13. Kim JY, An HG, Kim YW, Mitomo M (2000) J Mater Sci 35:3693. doi:10.1023/A:1004894906697
14. Sigl LS, Kleebe HJ (1993) J Am Ceram Soc 76:773
15. Volz E, Roosen A, Wang SC, Wei WCJ (2004) J Mater Sci 39:4095. doi:10.1023/B:JMSC.0000033388.55299.dc
16. Kim YW, Lee JH, Kim DY (2007) Mater Sci Forum 558–559:897
17. Kim Y-W, Lee SH, Nishimura T, Mitomo M (2005) Acta Mater 53:4701
18. Lawn BR, Padture NP, Cai H, Guiberteau F (1994) Science 263:1114
19. Guiberteau F, Padture NP, Lawn BR (1994) J Am Ceram Soc 77:1825
20. Lawn BR, Lee KS, Chai H, Pajares A, Kim DK, Wuttiphan S, Peterson IM, Hu X (2000) Adv Eng Mater 11:745
21. Lee KS, Jung YG, Peterson IM, Lawn BR, Kim DK, Lee SK (2000) J Am Ceram Soc 83:2255
22. Cai H, Kalceff MAS, Lawn BR (1993) J Mater Res 9:762
23. Lee SM, Kim TW, Yim HJ, Kim C, Kim YW, Lee KS (2007) J Ceram Soc Jpn 115:304
24. Hertz H (1896) Hertz's miscellaneous papers, chaps 5 and 6. Macmillan, London, UK
25. Lawn BR, Wilshaw TR (1975) J Mater Sci 10:1049. doi:10.1007/BF00823224
26. Guahk KH, Han IS, Lee KS (2008) Int J Mod Phys 22:1819
27. Kim Y-W, Lee YI (2003) Int J Mater Prod Technol 18:199
28. McColm IJ (1990) Ceramic hardness, 1st edn. Springer Press, USA
29. Lee CS, Lee KS, Lee S, Kim DK (2005) Key Eng Mater 287:421
30. Kim JH, Lee SW, Lee KS, Kim DK (2004) J Mater Sci 39:7023. doi:10.1023/B:JMSC.0000047547.09325.3d